White Rose
university consortium
Universities of Leeds, Sheffield & York

Reconstruction of a source domain from boundary measurements

B. Bin-Mohsin[1] and D. Lesnic[2]

[1]*Department of Mathematics, College of Science, King Saud University, PO. Box 2455 Riyadh 11451, Saudi Arabia*
[2]*Department of Applied Mathematics, University of Leeds, Leeds LS2 9JT, UK*
balmohsen@ksu.edu.sa, amt5ld@maths.leeds.ac.uk

Abstract

Inverse and ill-posed problems which consist of reconstructing the unknown support of a source from a single pair of exterior boundary Cauchy data are investigated. The underlying dependent variable, e.g. potential, temperature or pressure, may satisfy the Laplace, Poisson, Helmholtz or modified Helmholtz partial differential equations (PDEs). For constant coefficients, the solutions of these elliptic PDEs are sought as linear combinations of explicitly available fundamental solutions (free-space Greens functions), as in the method of fundamental solutions (MFS). Prior to this application of the MFS, the free-term inhomogeneity represented by the intensity of the source is removed by the method of particular solutions. The resulting transmission problem then recasts as that of determining the interface between composite materials. In order to ensure a unique solution, the unknown source domain is assumed to be star-shaped. This in turn enables its boundary to be parametrised by the radial coordinate, as a function of the polar or, spherical angles. The problem is nonlinear and the numerical solution which minimizes the gap between the measured and the computed data is achieved using the Matlab toolbox routine `lsqnonlin` which is designed to minimize a sum of squares starting from an initial guess and with no gradient required to be supplied by the user. Simple bounds on the variables can also be prescribed. Since the inverse problem is still ill-posed with respect to small errors in the data and possibly additional ill-conditioning introduced by the spectral feature of the MFS approximation, the least-squares functional which is minimized needs to be augmented with regularizing penalty terms on the MFS coefficients and on the radial function for a stable estimation of these couple of unknowns. Thorough numerical investigations are undertaken for retrieving regular and irregular shapes of the source support from both exact and noisy input data.

Keywords: Inverse problem; Method of fundamental solutions; Nonlinear optimization; Source domain identification.

1   Introduction

The determination of the support of a source contained in a given underlying medium from knowledge of the Cauchy data on the exterior boundary is investigated. As a practical procedure it resembles non-destructive testing of materials. Closely related to this inverse problem is that of detecting an unknown anomaly (defect) contained in a given domain from tomographic scaning on the skin/surface of the specimen under investigation. The inverse source problem investigated in this study is also closely related to the inverse potential gravimetry problem in which one is interested in determining the density inside the Earth from gravimetric measurements on its surface, see Novikov (1938) and Isakov (1990). Another possible application of our inverse source domain identification could be electroencephalography, see Jourhmane (1993), which is a non-invasive scanning tomographic technique of imaging/ measuring the electrical activity of the brain.

Prior to the present study, there were a few works which investigated the reconstruction of a source domain from boundary measurements from, mainly theoretical perspectives. The underlying medium was subject to various excitations such as electrical, i.e. Laplace's/Poisson's equation for the potential in electroencephalography, see Ito and Liu (2013) and Canelas *et al.* (2014), thermal, i.e. the modified Helmholtz equation for the temperature in a fin, see Mamud *et al.* (2014), or acoustics, i.e. the Helmholtz equation for the pressure, see Ikehata (1999).

In this paper, the aim is to reconstruct numerically in a stable and accurate manner the source domain entering all the aforementioned stationary elliptic fields. We employ a combined meshless technique with nonlinear optimization which recently has proved successful in a related study by the authors, see Bin-Mohsin and Lesnic (2014), concerned with the reconstruction of an inhomogeneity entering the modified Helmholtz equation.

We mention that for the potential field our problem and methodology is similar to that developed recently by Martins (2012). However, in our study we investigate Helmhholtz-type equations as well. We also do not avoid ill-conditioning by parameterising the unknown shape with a finite set of trigonometric polynomials, but rather keep the shape general and deal with it using regularization.

The plan of the paper is as follows. In Section 2, we introduce the mathematical formulation of the inverse source domain problem and state the available uniqueness results. In Section 3, we describe the MFS with the inhomogeneity removal, as well as the nonlinear minimization proposed for reconstructing the star-shape support of the unknown source. Section 4 presents and discusses thorough numerical results in which the convergence of the objective function with the number of iterations is analysed. Also, the stability of the numerical solution with respect to noise in the input data is investigated. Finally, Section 5 presents the conclusions of the work.

2   Mathematical formulation

We consider the inverse problem of determining an unknown source domain inhomogeneity Ω_2 compactly contained in a bounded domain $\Omega \subset \mathbb{R}^d$, $d = 2, 3$, appearing in the elliptic equation

$$\nabla^2 u + k^2 u = F_1 + (F_2 - F_1)\chi_{\Omega_2} \quad \text{in } \Omega, \tag{1}$$

where χ_{Ω_2} denotes the characteristic function of the domain Ω_2, $u \in H^1(\Omega)$ is the potential, $F_1, F_2 \in L^2(\Omega)$ are given source intensities which are assumed to be known and k is a known real or complex number or function. We assume that all the domains involved have a Lipschitz regularity boundary. From equation (1) one can observe that Ω_2 represents the support of the source function F_2 if $F_1 \equiv 0$.

By defining

$$u =: \begin{cases} u_1 & \text{in } \Omega_1 := \Omega \backslash \Omega_2, \\ u_2 & \text{in } \Omega_2, \end{cases} \tag{2}$$

equation (1) can be rewritten as the following transmission problem:

$$\nabla^2 u_1 + k^2 u_1 = F_1 \quad \text{in } \Omega_1, \tag{3}$$

$$\nabla^2 u_2 + k^2 u_2 = F_2 \quad \text{in } \Omega_2, \tag{4}$$

$$u_1 = u_2 \quad \text{on } \partial\Omega_2, \tag{5}$$

$$\frac{\partial u_1}{\partial n} = \frac{\partial u_2}{\partial n} \quad \text{on } \partial\Omega_2, \tag{6}$$

where n denotes the outward unit normal to the boundary. It might be also useful to remark that the right-hand side of equation (1) can be re-expressed as $F_1 \chi_{\Omega_1} + F_2 \chi_{\Omega_2}$.

Associated to (3)-(6) we also have prescribed one pair of Cauchy boundary data on $\partial\Omega$, namely,

$$u_1 = f \quad \text{on } \partial\Omega, \tag{7}$$

$$\frac{\partial u_1}{\partial n} = g \quad \text{on } \partial\Omega. \tag{8}$$

The inverse problem then requires the determination of the triplet solution $(u_1, u_2, \partial\Omega_2)$ satisfying equations (3)-(8). Such an important inverse problems arises in gravimetry, where one would like to determine the density of the Earth from the Cauchy data measurements of the gravity and its normal derivative on its surface. Other related obstacle identification problems and results in various fields are discussed by El-Badia and Ha-Duong (2000) and Isakov (2009).

The reconstruction of the source domain Ω_2 is nonlinear and ill-posed. One serious issue here is the uniqueness of solution from a single pair of Cauchy data (7) and (8). Unlike the inverse conductivity problem of electrical impedance tomography (EIT) in which the knowledge of the Dirichlet-to-Neumann map suffices to determine uniquely an isotropic conductivity, in the problem under investigation a single pair of Cauchy data contains all the information necessary for reconstruction, see Alves *et al.* (2009), in the sense that any other Cauchy data pair does not add any further information. Thus, one could take, without loss of generality, homogeneous Dirichlet data $f \equiv 0$ in (7) and non-identically zero Neumann data $0 \not\equiv g \in H^{-1/2}(\partial\Omega)$ in (8).

The following theorems give the classes of star-shaped, convex and polygonal obstacles for which uniqueness holds.

In the case of Laplace's/Poisson's equation, i.e. $k = 0$ in (1), we have the following uniqueness theorem in the class of star-shaped domains, see Isakov (1990, 2006), Hettlich and Rundell (1999), and Isakov *et al.* (2011).

Theorem 1. *Let $k = 0$ in (1). If F_1 and F_2 are given real constants, then the inverse problem (3)-(8) has at most one solution Ω_2 in the class of star-shaped domains with respect to their centre of gravity, i.e. barycentre.*

In the case of the modified Helmholtz equation, i.e. $k = ik'$ with $k' \in \mathbb{R}^*_+$ in (1), we have the following uniqueness theorem in the class of convex domains, see Isakov (1990) and Mamud *et al.* (2014).

Theorem 2. *Let $k = ik'$ with $k' \in \mathbb{R}^*_+$ in (1). If $F_1 \equiv 0$ and $F_2 > 0$, then the inverse problem (3)-(8) has at most one solution Ω_2 in the class of convex domains provided that, in addition, u is prescribed in an interior a priori known ball included in Ω_2.*
In the absence of this latter interior observation so far, one can only determine the centroid and the effective radius of Ω_2.

Finally, in the case of the Helmholtz equation, i.e. $k \in \mathbb{R}^*_+$ in (1), if $F_1 \equiv 0$, Ω_2 is a polygon and $0 \neq F_2 \in L^2(\Omega_2)$ is an unknown function which is locally Holder continuous with exponent $\alpha \in (0,1]$ in the neighbourhood of each vetex of $\partial\Omega_2$, then one can recover uniquely the convex hull $[\Omega_2]$ of Ω_2 in the problem (3)-(8), see Ikehata (1999).

Once the uniqueness of solution has been discussed, the next topic is to reconstruct the source domain Ω_2 numerically. Recently, the method of fundamental solutions (MFS) has proved, see Bin-Mohsin and Lesnic (2012, 2014), and Lesnic and Bin-Mohsin (2012), versatile and easy to use in detecting cavities, rigid inclusions and contact impedance obstacles, as well as inhomogeneities in inverse geometric problems governed by the modified Helmholtz equation. For a recent review of the MFS, as applied to solving inverse geometric problems, see Karageorghis *et al.* (2011). In this paper, we investigate yet another application of the MFS to reconstruct the source domain Ω_2 from the Cauchy data (7) and (8).

3 The method of fundamental solutions (MFS)

Prior to applying the MFS, we need to move the right-hand side source inhomogeneities F_1 and F_2 in (3) and (4) to the boundary conditions (5)-(8). This is done by finding particular solutions to (3) and (4), e.g. in the form of the Newton potential for Poisson's equation when $k = 0$, see Atkinson (1985). For the general case, we refer to the technique of Alves and Chen (2005), as well as to the references therein. However, as in our investigation the objective is to find the support Ω_2 of F_2 rather than its value which, in fact, is assumed to be known, we will consider the particular, but important, case, see Ito and Liu (2013) and Canelas *et al.* (2014), that F is piecewise constant within Ω, i.e. F_1 and F_2 are constants in (3) and (4). Without loss of generality, we can further assume that $F_1 = 0$ and $F_2 = 1$. Then, equations (3) and (4) become

$$\nabla^2 u_1 + k^2 u_1 = 0 \quad \text{in } \Omega_1, \tag{9}$$
$$\nabla^2 u_2 + k^2 u_2 = 1 \quad \text{in } \Omega_2. \tag{10}$$

We now decompose

$$u_2 = u_2^h + u_2^p, \tag{11}$$

where the homogeneous part u_2^h satisfies

$$\nabla^2 u_2^h + k^2 u_2^h = 0 \quad \text{in } \Omega_2, \tag{12}$$

and the inhomogeneous part is just a particular solution of equation (10) (in the whole $\mathbb{R}^d$) given by, see for example Jin and Zheng (2005),

$$u_2^p(x) = \frac{|x|^2}{2d}, \quad \text{if } k = 0, \tag{13}$$

$$u_2^p(x) = \frac{1}{k^2} + \begin{cases} I_0(-ik|x|) & \text{if } ik \in \mathbb{R}_-^* \\ J_0(k|x|) & \text{if } k \in \mathbb{R}_+^* \end{cases} \quad (x \in \mathbb{R}^2), \tag{14}$$

$$u_2^p(x) = \frac{1}{k^2} + \begin{cases} \frac{\sinh(-ik|x|)}{|x|} & \text{if } ik \in \mathbb{R}_-^* \\ \frac{\sin(k|x|)}{|x|} & \text{if } k \in \mathbb{R}_+^* \end{cases} \quad (x \in \mathbb{R}^3), \tag{15}$$

where of course, in the three-dimensional case the limits in (15) are equal to unity at the origin $x = 0$. Besides, the functions J_0 and I_0 denote the Bessel and the modified Bessel functions of the first kind of order 0, respectively. These special functions are analytical everywhere (including the origin) and in Matlab they are evaluated using routines `besselj(0,k*r)` (for J_0) and `besseli(0,k*r)` (for I_0).

With the superposition (11), the transmission interface conditions (5) and (6) become

$$u_1 = u_2^h + u_2^p \quad \text{on } \partial\Omega_2, \tag{16}$$

$$\frac{\partial u_1}{\partial n} = \frac{\partial u_2^h}{\partial n} + \frac{\partial u_2^p}{\partial n} \quad \text{on } \partial\Omega_2, \tag{17}$$

In (17), the normal derivatives of the particular solutions (13)-(15) are given by

$$\frac{\partial u_2^p}{\partial n}(x) = \frac{x \cdot n}{d}, \quad \text{if } k = 0, \tag{18}$$

$$\frac{\partial u_2^p}{\partial n}(x) = \begin{cases} -\frac{ikx \cdot n}{|x|} I_1(-ik|x|) & \text{if } ik \in \mathbb{R}_-^* \\ -\frac{kx \cdot n}{|x|} J_1(k|x|) & \text{if } k \in \mathbb{R}_+^* \end{cases} \quad (x \in \mathbb{R}^2), \tag{19}$$

$$\frac{\partial u_2^p}{\partial n}(x) = \begin{cases} \frac{(x \cdot n)}{|x|^2} \left[-ik \cosh(-ik|x|) - \frac{\sinh(-ik|x|)}{|x|} \right] & \text{if } ik \in \mathbb{R}_-^* \\ \frac{(x \cdot n)}{|x|^2} \left[k \cos(k|x|) - \frac{\sin(k|x|)}{|x|} \right] & \text{if } k \in \mathbb{R}_+^* \end{cases} \quad (x \in \mathbb{R}^3), \tag{20}$$

for $x \in \partial\Omega_2$, where J_1 and I_1 denote the Bessel and the modified Bessel functions of the first kind of order 1, respectively. They are evaluated using the routines `besselj(1,k*r)` (for J_1) and `besseli(1,k*r)` (for I_1).

Once the particular solution u_2^p has been prescribed as in (13)-(15), it can be removed from u_2 such that $u_2^h = u_2 - u_2^p$ satisfies the homogeneous equation (12). Then, we can apply the MFS for the composite material $\Omega = \Omega_1 \cup \Omega_2$ with $\Omega_1 \cap \Omega_2 = \emptyset$, as described in Berger and Karageorghis (1999) for the Laplace equation and in Bin-Mohsin and Lesnic (2011) for Helmholtz-type equations in layered materials. This consists of approximating the solutions u_1 and u_2^h of the elliptic homogeneous equations (9) and (12) by finite linear combinations of fundamental solutions of the form

$$u_{1,2N}(x) = \sum_{j=1}^{2N} a_j G_k(x, \xi_1^j), \quad x \in \overline{\Omega_1}, \tag{21}$$

$$u_{2,N}^h(x) = \sum_{j=1}^{N} b_j G_k(x, \xi_2^j), \quad x \in \overline{\Omega_2}, \tag{22}$$

where $\mathbf{a} = (a_j)_{j=\overline{1,2N}}$ and $\mathbf{b} = (b_j)_{j=\overline{1,N}}$ are unknown coefficients to be determined, $(\xi_1^j)_{j=\overline{1,2N}}$ are source points located outside the annular domain $\overline{\Omega_1}$, $(\xi_2^j)_{j=\overline{1,N}}$ are source points located outside the domain $\overline{\Omega_2}$, and G_k is the fundamental solution of the elliptic equation $\nabla^2 u + k^2 u = 0$ given by, see e.g. Alves and Chen (2005),

$$G_k(x, \xi) = \begin{cases} \ln|x - \xi| & \text{if } k = 0 \\ K_0(-ik|x - \xi|) & \text{if } ik \in \mathbb{R}_-^* \\ Y_0(k|x - \xi|) & \text{if } k \in \mathbb{R}_+^* \end{cases} \quad (x \in \mathbb{R}^2), \tag{23}$$

$$G_k(x, \xi) = \begin{cases} \frac{1}{|x-\xi|} & \text{if } k = 0 \\ \frac{\exp(-ik|x-\xi|)}{|x-\xi|} & \text{if } ik \in \mathbb{R}_-^* \\ \frac{\exp(ik|x-\xi|)}{|x-\xi|} & \text{if } k \in \mathbb{R}_+^* \end{cases} \quad (x \in \mathbb{R}^3), \tag{24}$$

where Y_0 and K_0 denote the Bessel and the modified Bessel functions of the second kind of order 0, respectively. These special functions have both a logarithmic singularity at the origin and are evaluated in Matlab using the routines `bessely(0,k*r)` (for Y_0) and `besselk(0,k*r)` (for K_0). One can avoid this singularity at the origin by employing the non-singular functions J_0 and I_0 in place of Y_0 and K_0, respectively, as in the boundary knot method (BKM) of Chen and Hon (2003). However, the meshless BKM, due to its spectral expansion character, it inherently introduces additional unwanted ill-conditioning and therefore, we do not follow this method here. Instead, we still use a meshless method, namely, the MFS but which by being based on the fundamental solution (23) (or (24)) it exhibits a singularity at the origin (when $|x-\xi| = 0$). The use of this fundamental solution is further justified rigorously through the denseness results of Bogomolny (1985) and Alves and Chen (2005). Moreover, for simplicity, we do not employ the complex version of the MFS for the Helmholtz equation in two-dimensions based on the Hankel function of the first kind of order zero, namely, $H_0^{(1)} = J_0 + iY_0$ because the singular character is still maintained in the imaginary part Y_0, see Ennenbach and Niemeyer (1996). The only slight difference, which in practice may happen very rarely, between using Y_0 instead of $H_0^{(1)}$ is when $Y_0(k|x - \xi|)$ may accidentally become very small giving poor or spurious numerical results, see Barnett and Betcke (2008). We remark that the normalisation constants usually appearing in the fundamental solution (23) (or (24)) have been omitted, as they were incorporated in the unknown coefficients $\mathbf{a}$ and $\mathbf{b}$ in (21) and (22), respectively. Finally, we mention that all the analysis of the section can easily be extended to include anisotropic homogeneous materials having as their leading part in (1) the anisotropic Laplace-Beltrami operator $\sum_{i,j=1}^{d} K_{ij} \frac{\partial^2 u}{\partial x_i \partial x_j}$, where $(K_{ij})_{i,j=\overline{1,d}}$ denotes the symmetric and positive conductivity tensor. The main change then is to replace the radial distance $|x|$ by the geodesic distance $x^T K^{-1} x$, see e.g. Jin and Chen (2006).

In what follows, for simplicity, we explain the inverse methodology in two-dimensions but a similar technique applies to three-dimensional problems as well, see Karageorghis *et al.* (2013).

The placement of source and collocation points is similar to that employed by Bin-Mohsin and Lesnic (2014), as follows. The source points $(\xi_1^j)_{j=\overline{1,N}} \notin \overline{\Omega}$ are placed on a (fixed) dilated pseudo-boundary $\partial\Omega'$ of similar shape as $\partial\Omega$. The remaining source points $(\xi_1^j)_{j=\overline{N+1,2N}} \in \Omega_2$ and $(\xi_2^j)_{j=\overline{1,N}} \notin \overline{\Omega_2}$ are placed on contraction and dilation (moving) pseudo-boundaries $\partial\Omega_2'$ and $\partial\Omega_2''$ similar to $\partial\Omega_2$ at a distance $\delta > 0$ in the inward and outward directions, respectively.

Without loss of generality, we may assume that the simply-connected domain Ω is the

unit circle $B(\mathbf{0}; 1)$. We also assume that the unknown support of the source F_2 is star-shaped with respect to the origin, i.e.

$$\partial\Omega_2 = \{r(\theta)(\cos(\theta), \sin(\theta))|\theta \in [0, 2\pi)\}, \tag{25}$$

where r is a 2π-periodic smooth function with values in $(0,1)$. The class of star-shaped domains is required for the uniqueness of a solution in the case $k = 0$ in Theorem 1, and it is also sufficiently general to model a wide range of shapes, e.g. circles, ellipses, rounded-rectangles, beans, acorns, kites, etc. that are usually tested in the inverse shape detection literature, see e.g. Ivanyshyn and Kress (2006), and Karageorghis and Lesnic (2009). In this setup of particular domains Ω and Ω_2, the collocation and source points are uniformly distributed as follows, see Bin-Mohsin and Lesnic (2014),

$$X_i = (\cos(\theta_i), \sin(\theta_i)), \quad X_{i+N} = r_i(\cos(\theta_i), \sin(\theta_i)), \quad i = \overline{1, N}, \tag{26}$$
$$\xi_1^j = R(\cos(\theta_j), \sin(\theta_j)), \quad \xi_1^{j+N} = (1 - \delta)X_{j+N}, \quad \xi_2^j = (1 + \delta)X_{j+N}, \quad j = \overline{1, N}, \tag{27}$$

where $\theta_i = 2\pi i/N$, $r_i := r(\theta_i)$ for $i = \overline{1, N}$, $R > 1$ and $\delta \in (0, 1)$.

The unknown radii vector $\mathbf{r} = (r_i)_{i=\overline{1,N}}$, characterising the star-shaped support Ω_2, together with the unknown MFS coefficients $\mathbf{a}$ and $\mathbf{b}$, giving the approximations of the solutions u_1 and u_2, are simulateneously determined by imposing the transmission conditions (16), (17) and the Cauchy data (7), (8) at the collocating points (26) in a least-squares sense. This results into minimizing the following (regularized) least-squares nonlinear objective function:

$$T(\mathbf{a}, \mathbf{b}, \mathbf{r}) := \left\|u_1 - f\right\|_{L^2(\partial\Omega)}^2 + \left\|\frac{u_1}{\partial n} - g^\epsilon\right\|_{L^2(\partial\Omega)}^2 + \left\|u_1 - u_2^h - u_2^p\right\|_{L^2(\partial\Omega_2)}^2$$
$$+ \left\|\frac{\partial u_1}{\partial n} - \frac{\partial u_2^h}{\partial n} - \frac{\partial u_2^p}{\partial n}\right\|_{L^2(\partial\Omega_2)}^2 + \lambda_1 \left\{\|\mathbf{a}\|^2 + \|\mathbf{b}\|^2\right\} + \lambda_2 \|\mathbf{r}'\|^2, \tag{28}$$

where λ_1, $\lambda_2 \geq 0$ are regularization parameters to be prescribed. These parameters are introduced in order to ensure/improve the stability of the nonlinear Tikhonov regularization functional (28). In (28), the Neumann data (8) was input as being a noisy perturbation g^ϵ of the exact data g in order to simulate the errors which are inherently present in any practical measurement. The last term in (28) represents a first-order derivative smoothness constraint on our desired shape for Ω_2, and is defined as:

$$\|\mathbf{r}'\|^2 = \sum_{i=1}^{N} \left(\frac{r_i - r_{i-1}}{\theta_i - \theta_{i-1}}\right)^2, \tag{29}$$

with the convention that $r_0 = r_N$ and $\theta_0 = 0$. Weighting/normalisation of the first 4 terms in (28) may be considered in order to avoid possible over-minimizations of individual terms but in our numerical experiments performed in Section 4 this was found unnecessary.

Introducing the MFS approximations (21) and (22) into (28) results in

$$T(\mathbf{a}, \mathbf{b}, \mathbf{r}) = \sum_{i=1}^{N} \left[\sum_{j=1}^{2N} a_j G_k(X_i, \xi_1^j) - f(X_i) \right]^2$$

$$+ \sum_{i=N+1}^{2N} \left[\sum_{j=1}^{2N} a_j \frac{\partial G_k}{\partial n}(X_{i-N}, \xi_1^j) - g^\epsilon(X_{i-N}) \right]^2$$

$$+ \sum_{i=2N+1}^{3N} \left[\sum_{j=1}^{2N} a_j G_k(X_{i-N}, \xi_1^j) - \sum_{j=1}^{N} b_j G_k(X_{i-N}, \xi_2^j) - u_2^p(X_{i-N}) \right]^2$$

$$+ \sum_{i=3N+1}^{4N} \left[\sum_{j=1}^{2N} a_j \frac{\partial G_k}{\partial n}(X_{i-2N}, \xi_1^j) - \sum_{j=1}^{N} b_j \frac{\partial G_k}{\partial n}(X_{i-2N}, \xi_2^j) - \frac{\partial u_2^p}{\partial n}(X_{i-2N}) \right]^2$$

$$+ \lambda_1 \left\{ \sum_{j=1}^{2N} a_j^2 + \sum_{j=1}^{N} b_j^2 \right\} + \lambda_2 \sum_{j=1}^{N} (r_j - r_{j-1})^2, \qquad (30)$$

where in the last term we have redenoted $\lambda_2/(2\pi/N)^2$ by λ_2.

The above minimization imposes $4N$ regularised equations in the $4N$ unknowns $(\mathbf{a}, \mathbf{b}, \mathbf{r})$. The noisy flux data g^ϵ is input as

$$g^\epsilon(X_i) = (1 + \rho_i \, p)g(X_i), \quad i = \overline{1, N}, \qquad (31)$$

where p represents the percentage of noise and ρ_i is a pseudo-random noisy variable drawn from a uniform distribution in $[-1, 1]$ using the MATLAB© command `-1+2*rand(1,N)`.

In equation (30), the normal derivative of G_k, via (23) and (24), is given by

$$\frac{\partial G_k}{\partial n}(x, \xi) = \begin{cases} \frac{(x-\xi)\cdot n}{|x-\xi|^2} & \text{if } k = 0 \\ \frac{ik(x-\xi)\cdot n}{|x-\xi|} K_1(-ik|x-\xi|) & \text{if } ik \in \mathbb{R}_-^* \\ -\frac{k(x-\xi)\cdot n}{|x-\xi|} Y_1(k|x-\xi|) & \text{if } k \in \mathbb{R}_+^* \end{cases} \quad (x \in \mathbb{R}^2) \qquad (32)$$

$$\frac{\partial G_k}{\partial n}(x, \xi) = \begin{cases} -\frac{(x-\xi)\cdot n}{|x-\xi|^3} & \text{if } k = 0 \\ \frac{(-ik|x-\xi|-1)\exp(-ik|x-\xi|)}{|x-\xi|^3}(x-\xi)\cdot n & \text{if } ik \in \mathbb{R}_-^* \\ \frac{(ik|x-\xi|-1)\exp(ik|x-\xi|)}{|x-\xi|^3}(x-\xi)\cdot n & \text{if } k \in \mathbb{R}_+^* \end{cases} \quad (x \in \mathbb{R}^3) \qquad (33)$$

where Y_1 and K_1 denote the Bessel and the modified Bessel functions of the second kind of order 1, respectively. These special functions have are evaluated using the routines `bessely(1,k*r)` (for Y_1) and `besselk(1,k*r)` (for K_1). In two-dimensions, i.e. $d = 2$, the normal n to the boundary $\partial\Omega_1$ is given by

$$n(X) = \begin{cases} (\cos(\theta), \sin(\theta)), & X \in \partial\Omega, \\ \frac{1}{\sqrt{r^2(\theta)+r'^2(\theta)}}(-r'(\theta)\sin(\theta) - r(\theta)\cos(\theta), r'(\theta)\cos(\theta) - r(\theta)\sin(\theta)), & X \in \partial\Omega_2. \end{cases} \quad (34)$$

In this formula, the derivative r' is approximated using finite differences as

$$r'(\theta_i) \approx \frac{r_i - r_{i-1}}{\theta_i - \theta_{i-1}}, \qquad i = \overline{1, N}. \qquad (35)$$

The routine `lsqnonlin` does not require the user to provide the gradient and, in addition, it offers the option of imposing lower and upper bounds on the elements of the vector of unknowns $(\mathbf{a}, \mathbf{b}, \mathbf{r})$ through the vectors `lb` and `ub`.

8

4 Numerical results and discussion

For simplicity, we consider numerical realisations in the two-dimensions only, with the three-dimensional case being deferred to future work. In all numerical experiments, the initial guess for the unknown vectors $\mathbf{a}$ and $\mathbf{b}$ are $\mathbf{0}$, and the initial guess for Ω_2 is a circle centred at the origin of radius 0.7. The Matlab toolbox routine `lsqnonlin` was run iteratively until a user-specified tolerance of $XTOL = 10^{-6}$ was achieved, or until when a user-specified maximum number of iterations $MAXCAL = 1000 \times 4N$ was reached. We have also set the simple bounds on the variable $(\mathbf{a}, \mathbf{b}, \mathbf{r})$ as the box $[-10^{10}, 10^{10}]^{2N} \times [-10^{10}, 10^{10}]^N \times (0, 1)^N$. The choices of the regularization parameters λ_1 and λ_2 in (30) were based on trial and error, but nevertheless more research work needs to be undertaken in the future on the rigorous selection of multiple regularization parameters, see e.g. Chen *et al.* (2008) and Belge *et al.* (2002).

In what follows, we take $k = 0$ for examples 1(a) and 2(a), $k' = 1$ for examples 1(b) and 2(b), and $k = 1$ for examples 1(c) and 2(c). In the subsequent figures 2–6 and 8–11, we graphically represent the initial guess by $(---)$, the numerical reconstruction by $(-\circ-)$ and the exact target by (——).

4.1 Example 1. (reconstructing a circular source domain)

We consider first retrieving a circle centred at the origin of radius $R_0 = 0.5$. That is, we seek the star-shape approximation (25) for the polar radius function

$$r(\theta) \equiv R_0 = 0.5, \quad \theta \in [0, 2\pi). \tag{36}$$

For the three cases of k that we consider we take the following examples with analytical solutions satisfying equations (9) and (10).

4.1.1 Example 1(a). ($k = 0$, Laplace's equation)

In the case $k = 0$, equations (9), (10) and (12) become

$$\nabla^2 u_1 = 0 \quad \text{in } \Omega_1, \tag{37}$$
$$\nabla^2 u_2 = 1 \quad \text{in } \Omega_2, \tag{38}$$
$$\nabla^2 u_2^h = 0 \quad \text{in } \Omega_2. \tag{39}$$

From (13) we also have that

$$u_2^p(r, \theta) = \frac{r^2}{4}, \quad (r, \theta) \in \mathbb{R}_+ \times [0, 2\pi). \tag{40}$$

We then take the analytical solutions of the equations (37)-(39) to be given by

$$u_1(r, \theta) = \frac{R_0^2}{2} \ln\left(\frac{r}{R_0}\right) + \frac{R_0^2}{4}, \quad (r, \theta) \in (R_0, 1) \times [0, 2\pi), \tag{41}$$

$$u_2(r, \theta) = \frac{r^2}{4}, \quad (r, \theta) \in (0, R_0) \times [0, 2\pi), \tag{42}$$

$$u_2^h(r, \theta) = 0, \quad (r, \theta) \in (0, R_0) \times [0, 2\pi). \tag{43}$$

9

Based on (41), the input Cauchy data (7) and (8) are given by

$$u_1(1, \theta) = f(\theta) = \frac{R_0^2}{2} \ln\left(\frac{1}{R_0}\right) + \frac{R_0^2}{4}, \quad \theta \in [0, 2\pi), \tag{44}$$

$$\frac{\partial u_1}{\partial n}(1, \theta) = g(\theta) = \frac{R_0^2}{2}, \quad \theta \in [0, 2\pi), \tag{45}$$

and, based on (25) and (40), the transmission interface conditions (16) and (17) become

$$u_1(r(\theta), \theta) = u_2^h(r(\theta), \theta) + \frac{r^2(\theta)}{4}, \quad \theta \in [0, 2\pi), \tag{46}$$

$$\frac{\partial u_1}{\partial n}(r(\theta), \theta) = \frac{\partial u_2^h}{\partial n}(r(\theta), \theta) + \frac{r(\theta)}{2}, \quad \theta \in [0, 2\pi). \tag{47}$$

From Theorem 1, we know that (36), (41) and (42) is the unique solution of the problem (37), (38), (44), (45), (5) and (6) in the class of star-shaped domains (25) with respect to the origin. In order to find this solution, we solve numerically, as described in Section 3, the inverse problem given by equations (37), (40), (44)-(47) to retrieve the analytical solution $(r(\theta), u_1(r, \theta), u_2^h(r, \theta))$ given by equations (36), (41) and (43). Also, once u_2^h has been obtained, equations (11) and (40) yield u_2.

4.1.2   Example 1(b). ($k = ik'$ with $k' \in \mathbb{R}_+^*$, modified Helmholtz equation)

In the case $k = ik'$ with $k' \in \mathbb{R}_+^*$, equations (9), (10) and (9) become

$$\nabla^2 u_1 - k'^2 u_1 = 0 \quad \text{in } \Omega_1, \tag{48}$$
$$\nabla^2 u_2 - k'^2 u_2 = 1 \quad \text{in } \Omega_2, \tag{49}$$
$$\nabla^2 u_2^h - k'^2 u_2^h = 0 \quad \text{in } \Omega_2. \tag{50}$$

From (13) we also have that

$$u_2^p(r, \theta) = -\frac{1}{k'^2} + I_0(k'r), \quad (r, \theta) \in \mathbb{R}_+ \times [0, 2\pi). \tag{51}$$

We then take the analytical solutions of the equations (48)-(50) to be given by

$$u_1(r, \theta) = B_0 K_0(k'r), \quad (r, \theta) \in (R_0, 1) \times [0, 2\pi), \tag{52}$$
$$u_2(r, \theta) = A_0 I_0(k'r) - 1, \quad (r, \theta) \in (0, R_0) \times [0, 2\pi), \tag{53}$$
$$u_2^h(r, \theta) = (A_0 - 1) I_0(k'r) - 1 + \frac{1}{k'^2}, \quad (r, \theta) \in (0, R_0) \times [0, 2\pi), \tag{54}$$

where

$$A_0 = \frac{K_1(k'R_0)}{I_0(k'R_0)K_1(k'R_0) + I_1(k'R_0)K_0(k'R_0)},$$
$$B_0 = -\frac{I_1(k'R_0)}{I_0(k'R_0)K_1(k'R_0) + I_1(k'R_0)K_0(k'R_0)}, \tag{55}$$

where we have used that $K_0' = -K_1$ and $I_0' = I_1$. Based on (52), the input Cauchy data (7) and (8) are given by

$$u_1(1, \theta) = f(\theta) = B_0 K_0(k'), \quad \theta \in [0, 2\pi), \tag{56}$$

$$\frac{\partial u_1}{\partial n}(1, \theta) = g(\theta) = -B_0 k' K_1(k'), \quad \theta \in [0, 2\pi), \tag{57}$$

10

and, based on (25) and (51), the transmission interface conditions (16) and (17) become

$$u_1(r(\theta), \theta) = u_2^h(r(\theta), \theta) + I_0(k'r(\theta)) - \frac{1}{k'^2}, \quad \theta \in [0, 2\pi), \tag{58}$$

$$\frac{\partial u_1}{\partial n}(r(\theta), \theta) = \frac{\partial u_2^h}{\partial n}(r(\theta), \theta) + k'I_1(k'r(\theta)), \quad \theta \in [0, 2\pi). \tag{59}$$

Then, we solve numerically, as described in Section 3, the inverse problem given by equations (48), (50), (56)-(59) to retrieve the analytical solution $(r(\theta), u_1(r, \theta), u_2^h(r, \theta))$ given by equations (36), (52) and (54). Also, once u_2^h has been obtained, equations (11) and (51) yield u_2.

4.1.3   Example 1(c).   ($k \in \mathbb{R}_+^*$, Helmholtz equation)

In the case $k \in \mathbb{R}_+^*$, we take the analytical solutions of equations (9), (10) and (12) to be given by

$$u_1(r, \theta) = D_0 Y_0(kr), \quad (r, \theta) \in (R_0, 1) \times [0, 2\pi), \tag{60}$$

$$u_2(r, \theta) = C_0 J_0(kr) + 1, \quad (r, \theta) \in (0, R_0) \times [0, 2\pi), \tag{61}$$

$$u_2^h(r, \theta) = (C_0 - 1)J_0(k'r) + 1 - \frac{1}{k^2}, \quad (r, \theta) \in (0, R_0) \times [0, 2\pi), \tag{62}$$

where

$$C_0 = \frac{Y_1(kR_0)}{Y_0(kR_0)J_1(kR_0) - Y_1(kR_0)J_0(kR_0)},$$

$$D_0 = \frac{J_1(kR_0)}{Y_0(kR_0)J_1(k'R_0) - Y_1(k'R_0)J_0(k'R_0)}, \tag{63}$$

where we have used that $Y_0' = -Y_1$ and $J_0' = -J_1$. From (13) we also have that

$$u_2^p(r, \theta) = \frac{1}{k^2} + J_0(kr), \quad (r, \theta) \in \mathbb{R}_+ \times [0, 2\pi). \tag{64}$$

Based on (60), the input Cauchy data (7) and (8) are given by

$$u_1(1, \theta) = f(\theta) = D_0 Y_0(k), \quad \theta \in [0, 2\pi), \tag{65}$$

$$\frac{\partial u_1}{\partial n}(1, \theta) = g(\theta) = -D_0 k Y_1(k), \quad \theta \in [0, 2\pi), \tag{66}$$

and, based on (25) and (64), the transmission interface conditions (16) and (17) become

$$u_1(r(\theta), \theta) = u_2^h(r(\theta), \theta) + J_0(kr(\theta)) + \frac{1}{k^2}, \quad \theta \in [0, 2\pi), \tag{67}$$

$$\frac{\partial u_1}{\partial n}(r(\theta), \theta) = \frac{\partial u_2^h}{\partial n}(r(\theta), \theta) - kJ_1(kr(\theta)), \quad \theta \in [0, 2\pi). \tag{68}$$

Then, we solve numerically, as described in Section 3, the inverse problem given by equations (9), (12), (65)-(68) to retrieve the analytical solution $(r(\theta), u_1(r, \theta), u_2^h(r, \theta))$ given by equations (36), (60) and (62). Also, once u_2^h has been obtained, equations (11) and (64) yield u_2.

11

Initially, we have performed several numerical runs with various values of the input MFS parameters and, for illustrative purposes, we have decided to show in figures 1–6 only a typical selected set of results obtained with $\delta = 0.5$, $R = 2$ and $N = 20$.

We consider first the case of exact data, i.e. $p = 0$ in equation (31). Figure 1 shows the unregularised nonlinear least-squares objective function (30) with $\lambda_1 = \lambda_2 = 0$, as a function of the number of iterations for examples 1(a)–1(c). From this figure it can be seen that a monotonic decreasing convergence is obtained for all examples. Furthermore, the convergence is faster for example 1(a) than for examples 1(b) and 1(c), but, at present, we have no explanation why this occurs.

In figure 2, we present the numerically reconstructed inner boundary for various numbers of iterations for no noise and no regularization for example 1(a). From this figure, it can be seen that the reconstructed inner source domain becomes accurate starting from 20 iterations up to 40 iterations. We also observe that as the number of iterations increases over 100, the reconstruction starts to be unstable and inaccurate.

We also add $p = 10\%$ noise in the flux g as in equation (31). The numerically obtained results for noise $p = 10\%$ with no regularization for various numbers of iterations for example 1(a) are shown in figure 3. From this figure, we note that the numerical solutions become less accurate as the number of iterations increases.

The corresponding regularized results obtained with different values of the regularization parameters $\lambda_1 = \lambda_2 \in \{10^{-9}, 10^{-6}, 10^{-3}\}$ after 500 iterations are shown in figures 4–6 for examples 1(a)–1(c), respectively. From these figures, we observe that $\lambda_1 = \lambda_2 = 10^{-3}$ yields the most accurate results for all Examples 1(a)–1(c).
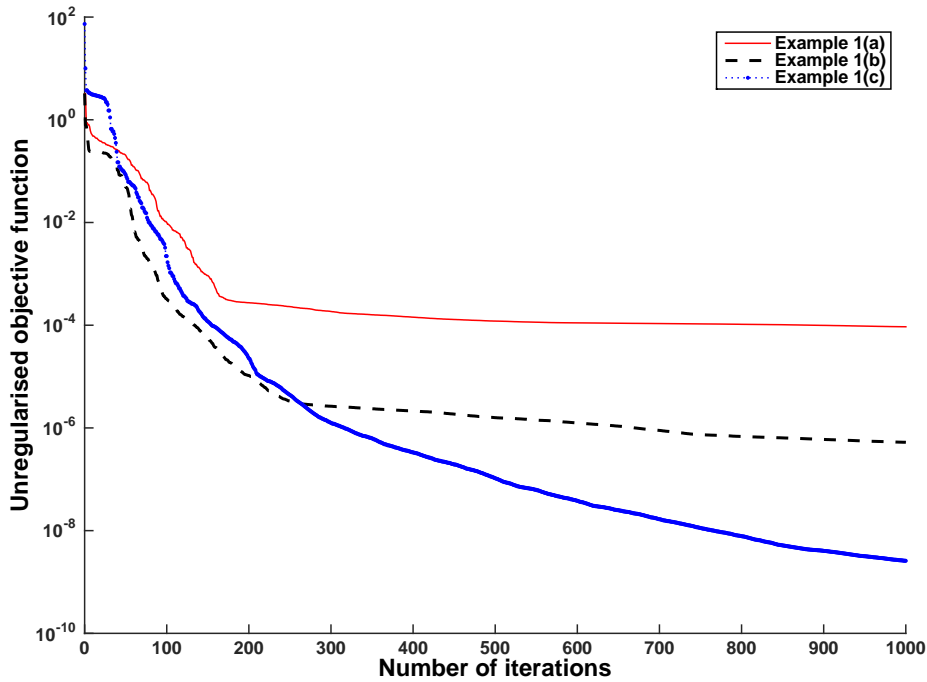

Figure 1: The unregularised objective function, as a function of the number of iterations, for no noise for examples 1(a)-1(c).
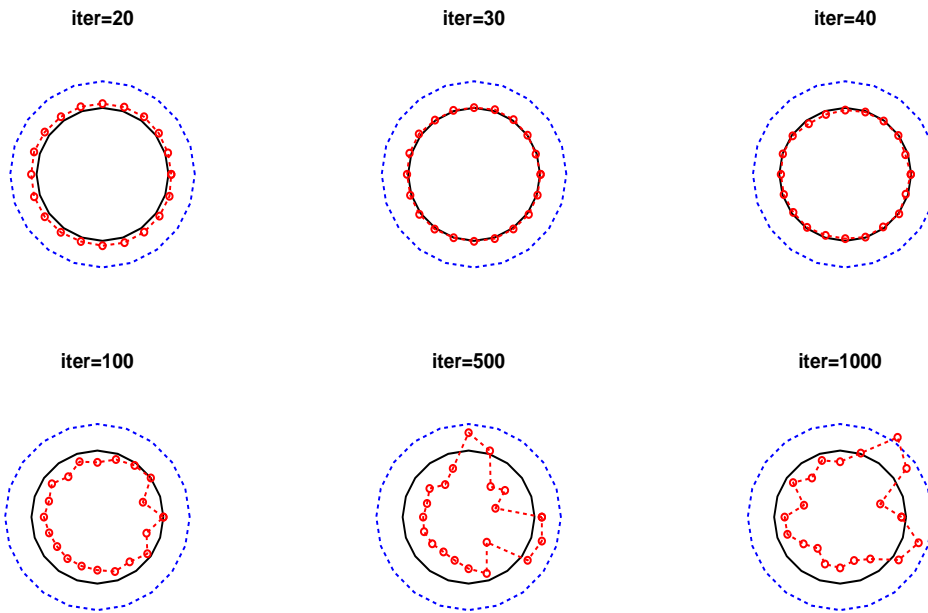
Figure 2: The reconstructed inner source domain for various numbers of iterations for no noise and no regularization, for example 1(a).
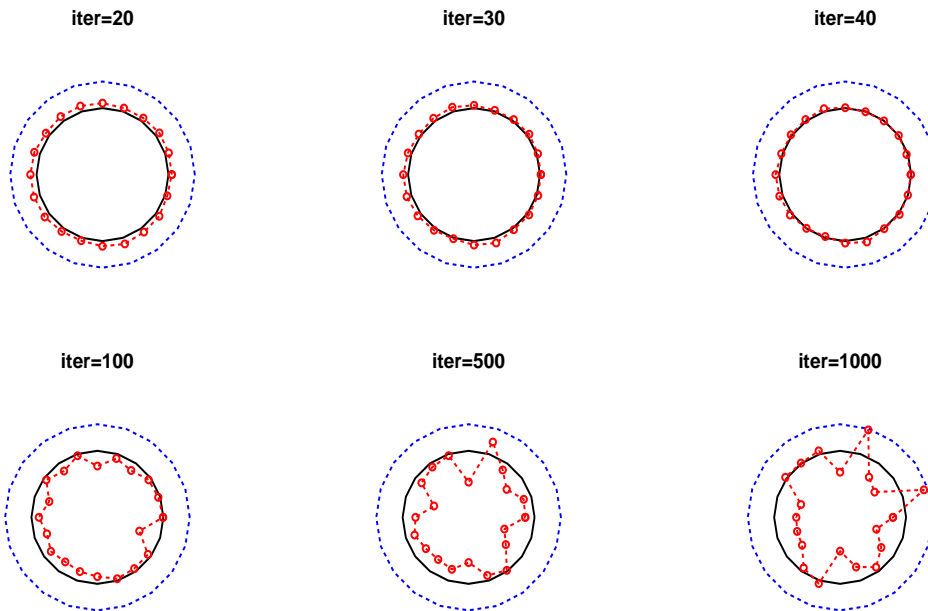

Figure 3: The reconstructed inner source domain for various numbers of iterations for $p = 10\%$ noise and no regularization, for example 1(a).
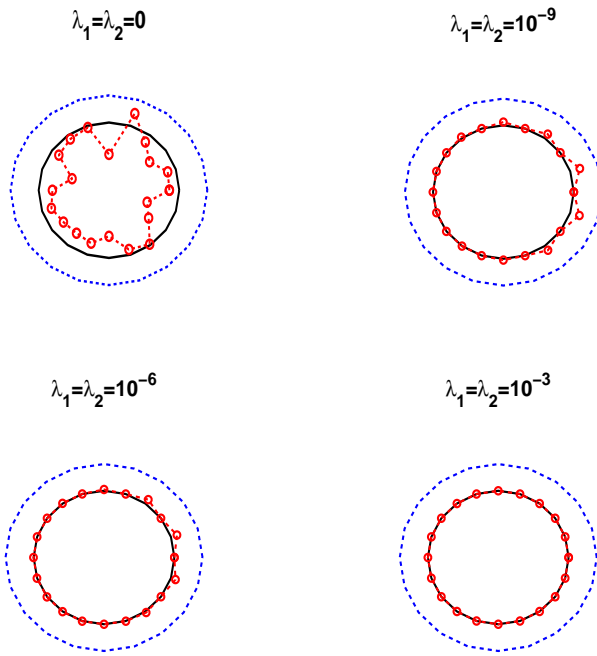
$\lambda_1=\lambda_2=0$

$\lambda_1=\lambda_2=10^{-9}$

$\lambda_1=\lambda_2=10^{-6}$

$\lambda_1=\lambda_2=10^{-3}$

Figure 4: The reconstructed inner source domain after 500 iterations for noise $p = 10\%$ and regularization, for example 1(a).
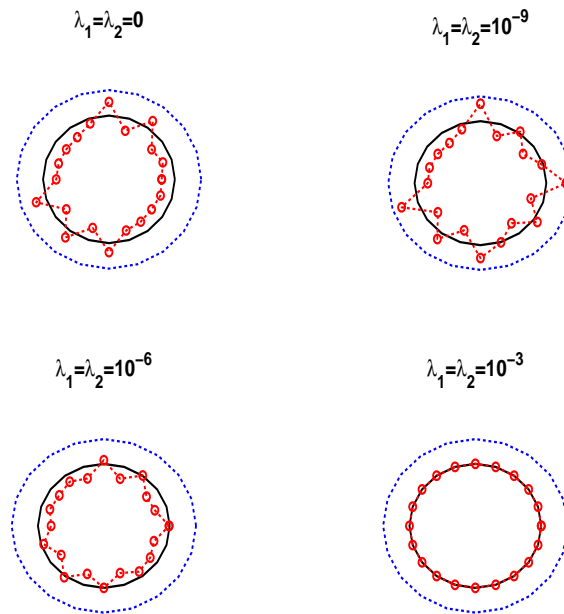
$\lambda_1=\lambda_2=0$

$\lambda_1=\lambda_2=10^{-9}$

$\lambda_1=\lambda_2=10^{-6}$

$\lambda_1=\lambda_2=10^{-3}$

Figure 5: The reconstructed inner source domain after 500 iterations for noise $p = 10\%$ and regularization, for example 1(b).
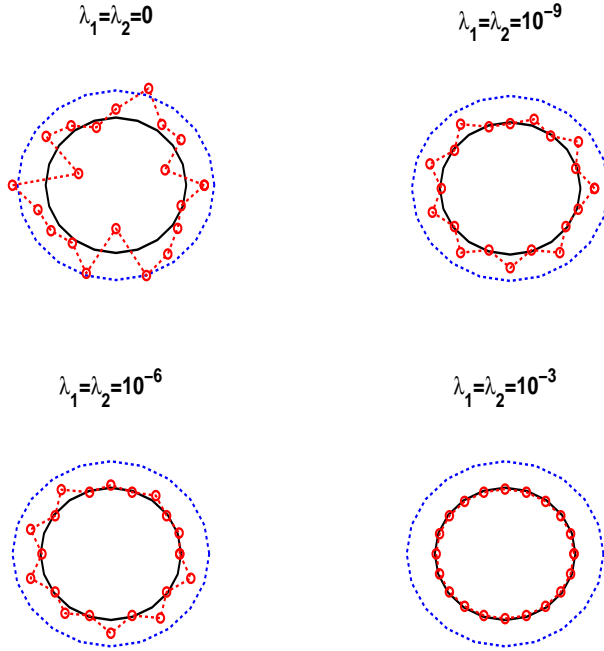
Figure 6: The reconstructed inner source domain after 500 iterations for noise $p = 10\%$ and regularization with, for example 1(c).

4.2 Example 2. (reconstructing a bean shape source domain)

As a second example we consider recovering a bean shape source domain given by the star-shape radial representation, see Bin-Mohsin and Lesnic (2014),

$$r(\theta) = \frac{0.5 + 0.4\cos(\theta) + 0.1\sin(\theta)}{1 + 0.7\cos(\theta)}, \qquad \theta \in [0, 2\pi). \tag{69}$$

In addition to being a more irregular shape to be retrieved than the previous simple circular shape (36), it also prevents analytical solutions for u being explicitly available. In this case, the Neumann data (8) is simulated numerically by solving first the direct problem given by equations (5), (6), (9), (10) and the Dirichlet data (7) given by

$$u_1(1, \theta) = f(\theta) = 0, \qquad \theta \in [0, 2\pi], \tag{70}$$

when the source domain Ω_2 is known and given by the star-shape representation (25) with the radial polar coordinate given by (69). Using the decomposition (11) in fact we solve (9), (12), (16), (17) and (70) using the MFS expansions (21) and (22) to determine the solutions u_1 and u_2^h. This recasts to solving the following linear system of $3N$ equations with $3N$ unknowns $\mathbf{a} = (a_j)_{j=\overline{1,2N}}$ and $\mathbf{b} = (b_j)_{j=\overline{1,2N}}$:

$$\sum_{j=1}^{2N} a_j G_k(X_i, \xi_1^j) = 0, \quad i = \overline{1, N}, \tag{71}$$

15

$$\sum_{j=1}^{2N} a_j G_k(X_i, \xi_1^j) - \sum_{j=1}^{N} b_j G_k(X_i, \xi_2^j) = u_2^p(X_i), \quad i = \overline{N+1, 2N}, \tag{72}$$

$$\sum_{j=1}^{2N} a_j \frac{\partial G_k}{\partial n}(X_{i-N}, \xi_1^j) - \sum_{j=1}^{N} b_j \frac{\partial G_k}{\partial n}(X_{i-N}, \xi_2^j) = \frac{\partial u_2^p}{\partial n}(X_{i-N}), \quad i = \overline{2N+1, 3N}. \tag{73}$$

In particular, the flux (8) is also of interest because it will be the overdetermined data in the inverse problem to be considered in the sequel. The normal derivative (8) is calculated by differentiating (21), namely

$$\frac{\partial u_{1,2N}}{\partial n}(x) = \sum_{j=1}^{2N} a_j \frac{\partial G_k}{\partial n}(x, \xi_1^j), \qquad x \in \partial\Omega, \tag{74}$$

where $\partial G_k / \partial n$ is expressed from equation (32). This is shown in figures 7(a)-(c) for $k = 0$, $k' = 1$ and $k = 1$, for $\delta = 0.3$, $R = 1.5$ and various degrees of freedom N. From these figures it can be seen that the numerical results are convergent, as the number of degrees of freedom increases. Twenty, respectively forty evenly spread points out of the curves $N = 40$ (for $k = 0$ and $k' = 1$), respectively, $N = 80$ (for $k = 1$) are chosen as Neumann numerically simulated data (8) in the inverse problem which is solved using $N = 20$ (for $k = 0$ and $k' = 1$), respectively, $N = 40$ (for $k = 1$).
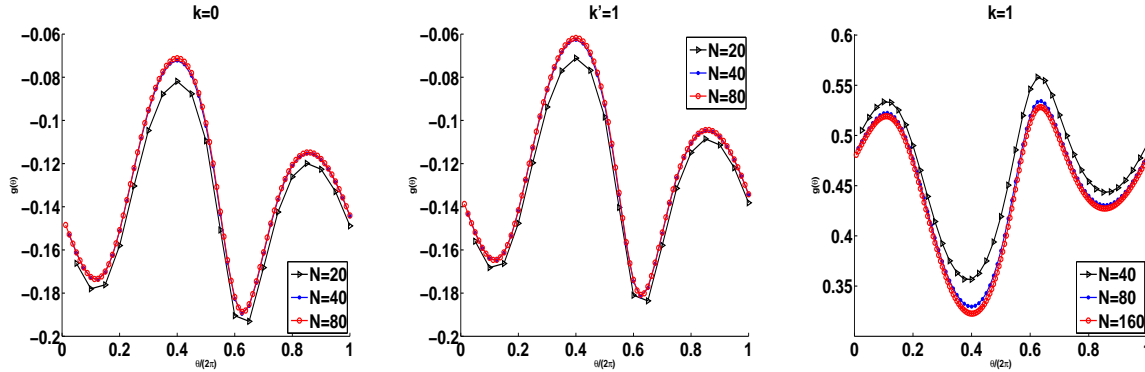

Figure 7: The normal derivative (8) obtained by solving the direct problem (9), (12), (16), (17) and (70) using the MFS with various values of N for $k = 0$, $k' = 1$ and $k = 1$.

Figures 8 - 11 for example 2 represent the same quantities as those contained in figures 3 - 6 for example 1 and similar conclusions can be observed, though, clearly, the reconstruction of the non-convex shape (69) is more involved than that of the simple circular shape (36).
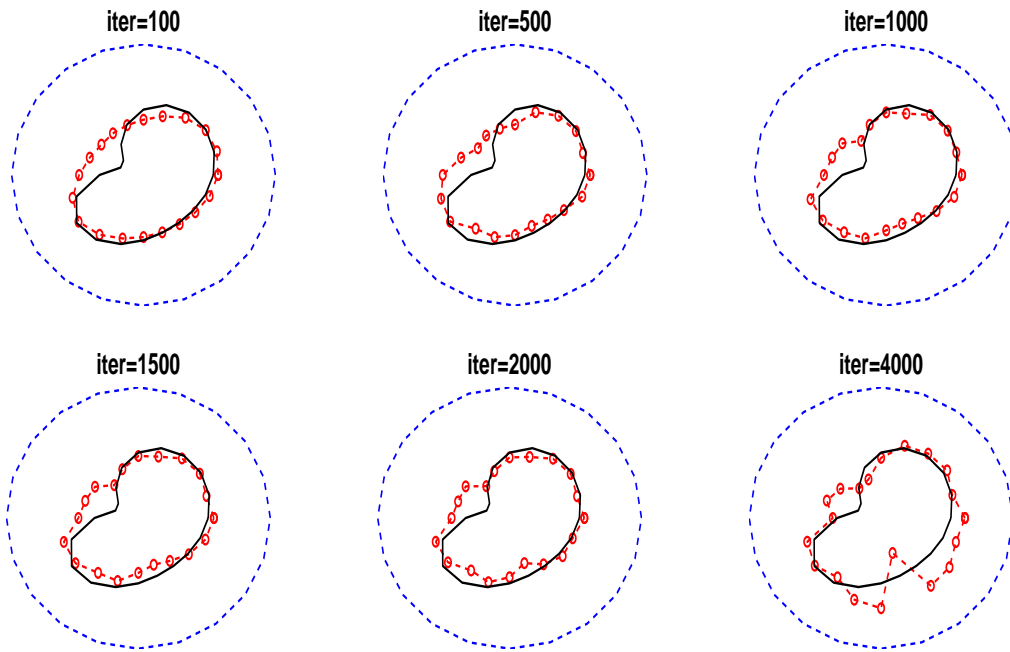
Figure 8: The reconstructed inner source domain for various numbers of iterations for $p = 10\%$ noise and no regularization, for example 2(a) with $k = 0$.
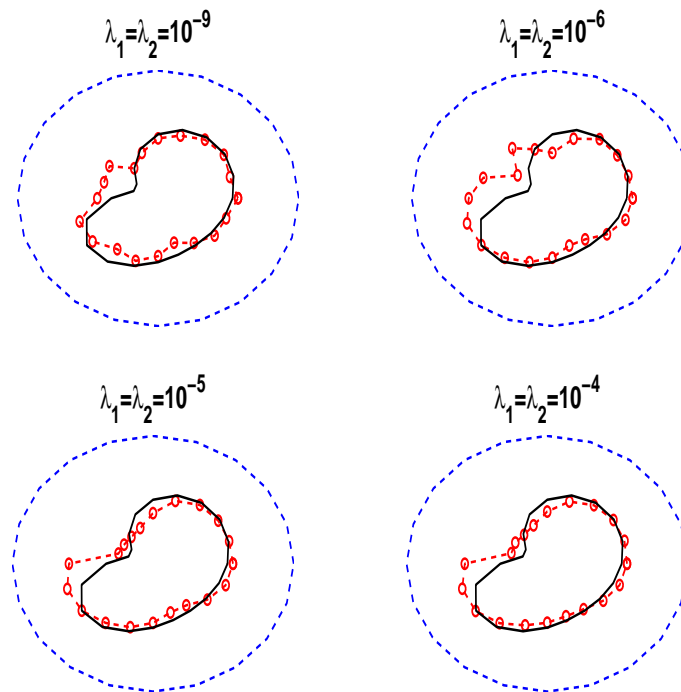

Figure 9: The reconstructed inner source domain after 2000 iterations for noise $p = 10\%$ and regularization, for example 2(a) with $k = 0$.
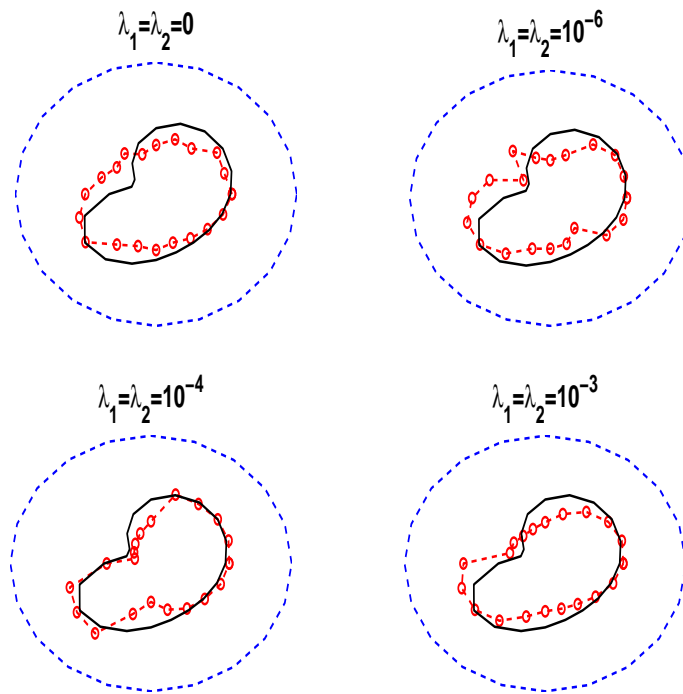
17

Figure 10: The reconstructed inner source domain after 500 iterations for noise $p = 10\%$ and regularization, for example 2(b) with $k' = 1$.
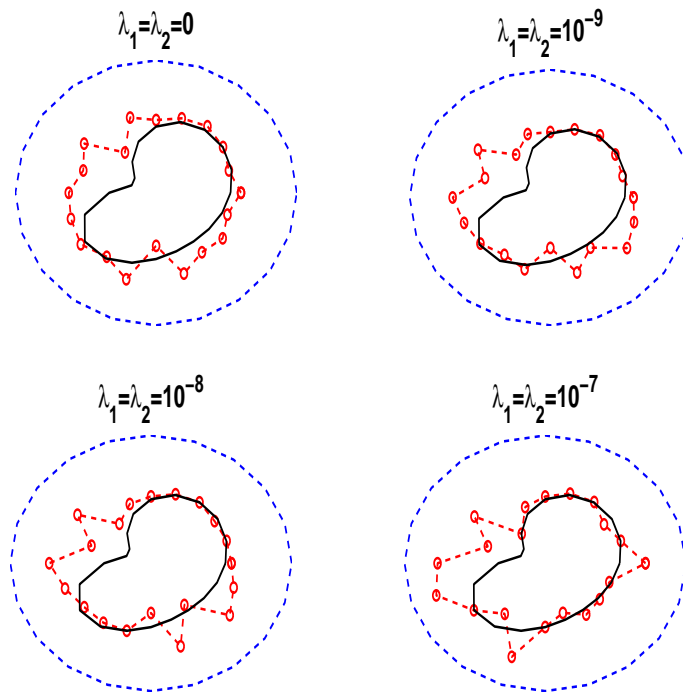

Figure 11: The reconstructed inner source domain after 500 iterations for noise $p = 10\%$ and regularization, for example 2(c) with $k = 1$.

5 Conclusions

In this paper, an inverse geometric problem which consists of reconstructing the unknown support of a source in the Poisson equation from a single pair of exterior boundary Cauchy data has been investigated using the MFS. Several examples have been investigated showing that the numerical results are satisfactory reconstructions for the unknown support of a source domain with reasonable stability against inverting noisy data. Regularization method has been used in order to obtain stable and accurate numerical results. Extensions to three-dimensional and time-dependent problems, see Harbrecht and Tausch (2011), will be the subject of a future work.

6 Acknowledgements

References

1. C.J.S. Alves and C.S. Chen (2005) A new method of fundamental solutions applied to nonhomogeneous elliptic problems, *Advances in Computational Mathematics* **23**, 125-142.

2. C.J.S. Alves, N.F.M. Martins and N.C. Roberty (2009) Full identification of acoustic sources with multiple frequencies and boundary measurements, *Inverse Problems and Imaging* **3**, 275-294.

3. K.E. Atkinson (1985) The numerical evaluation of particular solutions for Poisson's equation, *IMA Journal of Numerical Analysis* **5**, 319-338.

4. A.H. Barnett and T. Betcke (2008) Stability and convergence of the method of fundamental solutions for Helmholtz problems on analytic domains, *Journal of Computational Physics* **227**, 7003-7026.

5. M. Belge, M. Kilmer and E.L. Miller (2002) Efficient determination of multiple regularization parameters in a generalized L-curve framework, *Inverse Problems* **18**, 1161-1183.

6. J.R. Berger and A. Karageorghis (1999) The method of fundamental solutions for heat conduction in layered materials, *International Journal for Numerical Methods in Engineering* **45**, 1681-1694.

7. B. Bin-Mohsin and D. Lesnic (2011) The method of fundamental solutions for Helmholtz-type equations in composite materials, *Computers and Mathematics with Applications* **62**, 4377-4390.

8. B. Bin-Mohsin and D. Lesnic (2012) Determination of inner boundaries in modified Helmholtz inverse geometric problems using the method of fundamental solutions, *Mathematics and Computers in Simulation* **82**, 1445-1458.

9. A. Bogomolny (1985) Fundamental solutions method for elliptic boundary value problems, *SIAM Journal on Numerical Analysis* **22**, 644-669.

10. A. Canelas, A. Laurain and A.A. Novotny (2014) A new reconstruction method for the inverse potential problem, *Journal of Computational Physics* **268**, 417-431.

11. W. Chen and Y.C. Hon (2003) Numerical investigation on convergence of boundary knot method in the analysis of homogeneous Helmholtz, modified Helmholtz, and convection-diffusion problems, *Computer Methods in Applied Mechanics and Engineering* **192**, 1859-1875.

12. Z. Chen, Y. Lu, Y. Xu and H. Yang (2008) Multi-parameter Tikhonov regularization for linear ill-posed operator equations, *Journal of Computational Mathematics* **26**, 37-55.

13. A. El-Badia and T. Ha-Duong (2000) An inverse source problem in potential analysis, *Inverse Problems* **16**, 651-663.

14. R. Ennenbach and H. Niemeyer (1996) The inclusion of Dirichlet eigenvalues with singularity functions, *ZAMM* **76**, 377-383.

15. H. Harbrecht and J. Tausch (2011) An efficient numerical method for a shape identification problem arising from the heat equation, *Inverse Problems* **27**, 065013 (18 pages).

16. F. Hettlich and W. Rundell (1996) Iterative methods for the reconstruction of an inverse potential problem, *Inverse Problems* **12**, 251-266.

17. M. Ikehata (1999) Reconstruction of a source domain from the Cauchy data, *Inverse Problems* **15**, 637-643.

18. V. Isakov (1990) *Inverse Source Problems*, Mathematical Surveys and Monographs, Vol.**34**, Providence, RI, American Mathematical Society.

19. V. Isakov (2006) *Inverse Problems for Partial Differential Equations*, 2nd edn., Springer, New York.

21. V. Isakov, S. Leung and J. Qian (2011) A fast local level set method for inverse gravimetry, *Communications in Computational Physics* **10**, 1044-1070.

22. K. Ito and J.-C. Liu (2013) Recovery of inclusions in 2D and 3D domains for Poisson's equation, *Inverse Problems* **29**, 075005 (19 pages).

23. O. Ivanyshyn and R. Kress (2006) Nonlinear integral equations for solving inverse boundary value problems for inclusions and cracks, *Journal of Integral Equations and Applications* **18**, 13-38.

24. B. Jin and Y. Zheng (2005) Boundary knot method for some inverse problems associated with the Helmhholtz equation, *International Journal for Numerical Methods in Engineering* **62**, 1636-1651.

25. B. Jin and W. Chen (2006) Boundary knot method based on geodesic distance for anisotropic problems, *Journal of Computational Physics* **215**, 614-629.

26. M. Jourhmane (1993) *Methodes Numeriques de Resolution d'un Probleme d'Electroencephalographie*, PhD Thesis, Universite de Rennes I, France.

27. A. Karageorghis and D. Lesnic (2009) Detection of cavities using the method of fundamental solutions, *Inverse Problems in Science and Engineering* **17**, 803-820.

28. A. Karageorghis, D. Lesnic and L. Marin (2011) The MFS for inverse geometric problems, *Inverse Problems and Computational Mechanics*, Vol.**1**, (eds. L. Marin, L. Munteanu and V. Chiroiu), Editura Academiei, Bucharest, Romania, Chapter **8**, pp.191-216.

29. A. Karageorghis, D. Lesnic and L. Marin (2013) A moving pseudo-boundary MFS for three-dimensional void detection, *Advances in Applied Mathematics and Mechanics* **5**, 510-527.

30. D. Lesnic and B. Bin-Mohsin (2012) Inverse shape and surface heat transfer coefficient identification, *Journal of Computational and Applied Mathematics* **236**, 1876-1891.

31. R.G.S. Mamud, N.C. Roberty and C.J.S. Alves (2014) Analytical observability of symmetric star shaped sources for modified Helmholtz model, *8th International Conference on Inverse Problems in Engineering*, May 12-15, 2014, Poland, (eds. I. Szczygiel, A.J. Nowak and M. Rojczyk), pp.179-188.

32. N.F.M. Martins (2012) An iterative shape reconstruction of source functions in potential problem using the MFS, *Inverse Problems in Science and Engineering* **20**, 1175-1193.

33. P. Novikov (1938) Sur le probleme inverse du potential, *Doklady Akad. Nauk* **18**, 165-168.